Model for the insulating behavior of Pb- or K-doped $BaBiO_3$

U. Hahn, G. Vielsack,* and W. Weber
Institut für Physik, Universität Dortmund, D-44227 Dortmund, Germany
(Received 15 November 1993)

A simple model is presented to describe the nonmetallic behavior observed over wide doping ranges of perovskite-type $BaBi_{1-x}Pb_xO_3$ and $Ba_{1-x}K_xBiO_3$ alloys. The model is based on the idea that the oxygen octahedra endure static distortion waves of a "breathing" type, with wave vectors $\mathbf{Q}(x)$ nesting to the respective alloy Fermi surfaces as obtained from the energy bands of a virtual-crystal band model. For $BaBi_{1-x}Pb_xO_3$, Bi-Pb ordering waves are added by placing the Bi atoms onto those octahedral sites that exhibit the largest breathing distortions. Using a simple tight-binding Hamiltonian based on realistic energy-band calculations, the model has been studied on large supercells, testing a multitude of lattice configurations. Experimental consequences are discussed.

I. INTRODUCTION

Upon doping, the bismuthate system $BaBiO_3$ of perovskite-type lattice remains nonmetallic up to much larger dopant concentrations than the corresponding cuprates. For $(Ba_{1-x}K_x)BiO_3$, a metallic (and superconducting) behavior is found only for $x \gtrsim 0.3$,[1,2] while the nonmetallic phase of $Ba(Bi_{1-x}Pb_x)O_3$ ranges even up to $x \approx 0.65$.[3] In the cuprates, on the other hand, the CuO_2 planes become metallic for dopant concentrations as small as $x \approx 0.05 - 0.10$. In a one-electron approximation for the electronic structure, and assuming one formula unit per unit cell, pure $BaBiO_3$ should also be metallic — a half-filled band situation similar to La_2CuO_4 or $YBa_2Cu_3O_6$. However, a commensurate charge-density wave (CDW) instability is present in $BaBiO_3$, manifest by alternating "breathing" type distortions of the O octahedra, which surround the Bi ions.[4] These O displacements lead to two inequivalent Bi sites. They can also be described as a result of a charge disproportionation of the Bi^{4+} ions leading to a formula unit of $Ba_2Bi^{4+\Delta}Bi^{4-\Delta}O_6$. In contrast to the insulating cuprates, no antiferromagnetism is found in $BaBiO_3$.

Doped $BaBiO_3$ does not exhibit two crystallographically inequivalent Bi sites.[5,6] Optical and transport data are available, especially for the nonmetallic part of the $Ba(Bi,Pb)O_3$ system, where growth of single crystals has been achieved. An optical gap appears to be present over almost the whole Pb-Bi alloy range, even in the metallic region, decreasing monotonously from $E_G \approx 2$ eV for $BaBiO_3$ to $E_G \approx 0.2$ eV for $x \approx 0.8$.[7,8] The conductivity gap, derived from the temperature dependence of the resistivity, is much smaller ($E_C^{\max} \approx 0.3$ eV) but changes in a similar way.[8] The optical data have been interpreted as a gap structure "riding on the (shifting) Fermi energy."[9]

In energy-band theory using local-density approximation (LDA), the half-filled conduction band of $BaBiO_3$ is the antibonding part of a band complex built mainly of the Bi $6s$ and the O $2p_\sigma$ orbitals.[10] These hybrid bands spread over a wide energy range $W \approx 16$ eV, because of the very large $sp\sigma$ energy-transfer (hopping) matrix elements ($t_{sp\sigma} \approx 2.2$ eV) and almost degenerate orbital energies ($E_p - E_s \approx 2 - 6$ eV). At half filling, the shape of the Fermi surface allows a very effective nesting for the zone boundary wave vector $\mathbf{Q} = 2\mathbf{k}_F = \frac{\pi}{a}(1,1,1)$. Breathing-type distortions of the O octahedra open large gaps of order 1 eV over the complete Fermi surface.[11] Other distortions, however, such as octahedral rotations (which are also present in the real $BaBiO_3$ structure), or alternating quadrupolar deformations of the octahedra, lead only to very small changes of the states near the Fermi energy E_F.[10]

Upon doping, one would expect a rigid band picture to hold — especially for alkali-doped $BaBiO_3$.[12] Then, the Fermi vectors k_F should contract, leading to incommensurate CDW wave vectors. As a consequence, local gaps are expected for those states at E_F, where nesting can be achieved. Yet it is not clear whether a global gap at E_F can be opened by the distortion waves. In earlier work, a model has been briefly sketched, which attributes the wide nonmetallic range in the phase diagram of $Ba(Bi_{1-x}Pb_x)O_3$ to the presence of both charge-density waves and ordering waves in the Pb-Bi lattice.[13]

In this paper we present a detailed study of this model, and also a corresponding model for alkali-doped $BaBiO_3$. A brief report on some results of this study has been given in Ref. 14. Our model employs a simple tight-binding Hamiltonian derived from LDA energy-band calculations (see Sec. II). Using a superlattice technique we investigate a large number of lattice configurations, which are constructed to provide both breathing-type charge-density wave distortions and Pb-Bi ordering waves. The wave vectors $\mathbf{Q} \approx 2\mathbf{k}_F$ are chosen as to agree with the respective dopant concentration x. The construction of the supercell configurations is outlined in Sec. III. Numerical results are presented and discussed in Sec. IV. Concluding remarks are given in Sec. V.

II. HAMILTONIAN

In order to study as big supercells as possible, we have used the minimum basis set tight-binding Hamiltonian

proposed by Mattheiss and Hamann,[10] where only the $6s$ orbitals of Bi or Pb and the $2p_\sigma$ orbitals of O were employed. The hopping is limited to the nearest-neighbor matrix element $t_{sp\sigma}$. The values for the matrix elements are[10]

$$\varepsilon_p(\mathrm{O}) = 0, \quad \varepsilon_s(\mathrm{Bi}) = -6 \text{ eV}, \quad \varepsilon_s(\mathrm{Pb}) = -2 \text{ eV}$$

and for the hopping matrix elements, allowing the O atoms to displace along the respective bonds ($\pm\delta \approx 0.1$ Å) :

$$t_{sp\sigma} = 2.2 \text{ eV} \pm \beta\delta \text{ with } \beta = 2.0 \text{ eV/Å}.$$

This Hamiltonian will lead to four energy bands per formula unit, the bonding $6s$-$2p$ band being the lowest, and the antibonding one being the highest in energy. In between, there are two nonbonding O 2p bands, dispersionless and degenerate. These states remain unaffected by any of the breathing-type distortions investigated in our study. It is always possible to block diagonalize the supercell Hamiltonian in order to eliminate the nonbonding states (see the Appendix). The structure of the antibonding band, including the effects of the breathing distortion, is shown in Fig. 1.

Apart from the change of $t_{sp\sigma}$ with the O displacements, it is also possible that the orbital energies ε_s(Bi) or ε_s(Pb) shift due to the breathing distortions. In fact, from results of detailed LDA energy-band calculations for distorted $BaBiO_3$ it has been found that these shifts are rather large ($\approx \pm 1$ eV).[15,16] This result became available during the course of our study and has been implemented in particular for the $(Ba_{1-x}K_x)BiO_3$ calculations. There we have used

$$\varepsilon_s(\mathrm{Bi}) = -4.9 \text{ eV} \pm \beta'\delta, \quad t_{sp\sigma} = 2.2 \text{ eV} \pm \beta\delta$$

with

$$\beta' = 10 \text{ eV/Å} \text{ and } \beta = 1.5 \text{ eV/Å}.$$

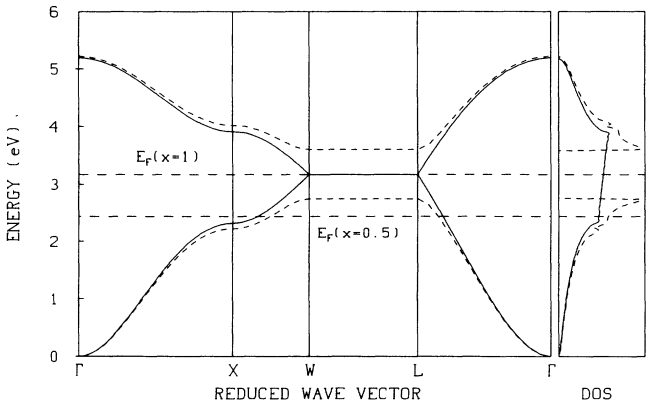

FIG. 1. Antibonding band of $BaBiO_3$ calculated with the tight-binding model of Sec. II. The fcc Brillouin zone of breathing-distorted $BaBiO_3$ is used to demonstrate the band splitting at E_F due to the $\frac{\pi}{a}(1,1,1)$ CDW (dashed lines). The solid lines depict the (backfolded) undistorted band. Further shown are the respective density of states curves. The Fermi level for $x = 0.5$ is also indicated.

Note the slightly modified orbital energy ε_s(Bi). No Ba or K orbitals are incorporated, since there is hardly any admixture of such orbitals in the conduction band.[12]

III. CONSTRUCTION OF SUPERCELL CONFIGURATIONS

The simplest superstructure which provides a gap at E_F is the alternating breathing distortion of the O octahedra in pure $BaBiO_3$ (see Fig. 1). We can associate a wave vector $\mathbf{Q} = 2\mathbf{k}_F = (1,1,1)$ to this CDW, and displacements along the α direction

$$d_{i\alpha}(\mathbf{Q}) = Q_\alpha \cos(\mathbf{Q}\mathbf{R}_i) \tag{1}$$

for O atoms at sites $\mathbf{R}_i$ and bonding along the α direction (from now on all wave vectors are given in units of $\frac{\pi}{a}$).

We now consider a wave vector $\mathbf{Q} = (1,0,1)$ (which would correspond to $|\mathbf{Q}| \approx 2k_F$ for a doping value of $x = 0.5$). The respective breathing displacements $d_{i\alpha}(\mathbf{Q})$ are then planar; i.e., all O atoms bonding to Bi atoms along the x or z axes move, yet the O atoms bonding along the y axis remain at their half-way positions. It is now possible to add the displacements of another member of the star $\{\mathbf{Q}\}$, e.g., $\mathbf{Q}_2 = (0,1,1)$. In doing so, one realizes that each displacement wave $d_{i\alpha}(\mathbf{Q})$ associated with the member n of the star $\{\mathbf{Q}\}$ may have a relative phase ϕ_n. Thus we have to modify Eq. (1) to

$$d_{i\alpha}(\mathbf{Q}_n, \phi_n) = Q_\alpha \cos(\mathbf{Q}_n\mathbf{R}_i + \phi_n). \tag{2}$$

When we superpose various displacements $d_{i\alpha}$, we may also allow for a variation of the amplitudes A_n of the different waves. Finally, it is conceivable to mix adjacent $|\mathbf{Q}|$ waves, that is, e.g., to mix the $\mathbf{Q}_n$ of $\{1,1,\frac{2}{3}\}$ and $\{1,1,1\}$.

It is clear, however, that the total displacement

$$d_{i\alpha}^{\mathrm{tot}} = \sum_n A_n d_{i\alpha}(\mathbf{Q}_n, \phi_n) \tag{3}$$

should not exceed a certain critical value, since large anharmonic effects are expected to limit the distortions of the Bi—O bonds, which are the strongest in the lattice. Therefore, we used the following expression for the actual O displacements in our supercell configurations

$$\delta_{i\alpha} = \delta \tanh[r\, d_{i\alpha}^{\mathrm{tot}}/d_{\mathrm{max}}^{\mathrm{tot}}], \tag{4}$$

where $d_{\mathrm{max}}^{\mathrm{tot}}$ is the largest value of $|d_{i\alpha}^{\mathrm{tot}}|$ in a given configuration $d_{i\alpha}^{\mathrm{tot}}$. This procedure allows to study not only the square-wave approximation $r \to \infty$ (replacing tanh by sign, as used in Ref. 13), but also more realistic distributions of O distortions, when $r \approx 5, \ldots, 10$ is chosen.

As an example we give now a configuration for $x = 0.5$ constructed by superposing displacements $d_{i\alpha}$ with wave vectors $\mathbf{Q} = (1,0,1)$ and $\mathbf{Q} = (0,1,1)$, phases $\phi_{1,2} = 0$ and equal amplitudes $A_{1,2}$. The supercell is $2 \times 2 \times 2$ (see Fig. 2). Having constructed one such configuration $\{A_n, \mathbf{Q}_n, \phi_n\}$ in a certain supercell, the next problem is to distribute the Bi and Pb atoms on the sites j of the

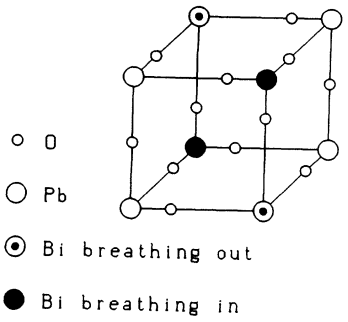

FIG. 2. The nonmetallic $2\times2\times2$ configuration for $x = 0.5$.

Bi/Pb sublattice. For this purpose we first analyze all sites j according to their "breathing character." This is measured by a number n_{Br}, which can take all values between -6 and $+6$. Here $+6$ corresponds to the case where all O atoms i around site j have fully moved inward, and -6 to the case of full outward motion. Values of $|\ n_{\mathrm{Br}}\ | < 6$ represent sites where either not all of the O atoms have moved, or some have moved inward and others outward, etc.

The dopant concentration x determines the number of Bi sites in each supercell configuration $\{A_n, \mathbf{Q}_n, \phi_n\}$. The Bi atoms were put on those sites j with maximum breathing character $n_{\mathrm{Br}} = \pm6$, and, in some configurations, at sites with $n_{\mathrm{Br}} = \pm5$ or $n_{\mathrm{Br}} = \pm4$. In our example of Fig. 2, there are four sites with $n_{\mathrm{Br}} = \pm6$ and another four sites with $n_{\mathrm{Br}} = 0$. By putting the Bi atoms on the four sites $n_{\mathrm{Br}} = \pm6$, and the Pb atoms on the other sites, we can achieve the concentration $x = 0.5$.

Consider now as a counter example the case where the three vectors

$$(1,1,0),\quad (1,0,1),\quad \text{and}\quad (0,1,1)$$

are superposed with phases $\phi_n = 0$. One finds two sites with $n_{\mathrm{Br}} = +6$ and six sites with $n_{\mathrm{Br}} = -2$. It is not possible to distribute the Bi atoms in a unique way. Configurations like these were dismissed. We note that test calculations for such configurations never displayed gaps at the Fermi energy (see also Sec. IV A).

The example of Fig. 2 was constructed using a $2\times2\times2$ supercell. In order to investigate many more configurations, we have also used wave vectors $\mathbf{Q}$ with components 1/2, 1/3, and 2/3. Consequently, the size of the supercell had to be increased to $4\times4\times4$ (corresponding to a dimension of the Hamilton matrix of $d = 256$, reduced by block diagonalization to $d_r = 128$), and to $6\times6\times6$, respectively ($d_r = 432$). In some cases, $n^2\times2$ with $n = 4, 6, 8$ configurations were also investigated. The resulting Brillouin zones were orthorhombic, in general. To find out whether, for a certain configuration, a gap existed at E_F, the eigenvalues of the Hamilton matrix had to be calculated for at least eight k points (Γ point and seven zone-boundary points). The density of states curves have been calculated using up to 216 k points in the irreducible wedge.

IV. RESULTS AND DISCUSSION

A. The limit of isolated clusters

We consider first a limiting case, where the O displacements are very large, leading either to strongly enhanced Bi-O (Pb-O) hopping or to strongly suppressed hopping. As an example we have chosen $t_{sp\sigma}^{\mathrm{short}} \Rightarrow 2t_{sp\sigma} = 4.4$ eV and $t_{sp\sigma}^{\mathrm{long}} \Rightarrow 0$. In this case there exist only isolated clusters of O atoms around the Pb or Bi atoms (apart from some configurations where O atoms between two Pb atoms do not displace). For these isolated clusters the energy levels are given by the expression

$$\varepsilon_{\pm} = \frac{1}{2}\left[\varepsilon(\mathrm{Bi,Pb}) + \varepsilon(\mathrm{O}) \pm \sqrt{\Delta\varepsilon(\mathrm{Bi,Pb})^2 + 8\,(n_{\mathrm{Br}} + 6)\,t_{sp\sigma}^2}\ \right]$$

with n_{Br} being the breathing character of the cluster (see Fig. 3) and $\Delta\varepsilon(\mathrm{Bi,Pb}) = \varepsilon(\mathrm{Bi,Pb}) - \varepsilon(\mathrm{O})$. Note that the lowest antibonding level is $\varepsilon_+ = 0$ (for $n_{\mathrm{Br}} = -6$), degenerate with the nonbonding O levels. Because of the small $\Delta\varepsilon(\mathrm{Pb})$, the level spacing for $\varepsilon_+(\mathrm{Pb})$ is considerably larger than for $\varepsilon_+(\mathrm{Bi})$, especially for the low-lying levels.

Each level can host two electrons. By placing the Bi atoms on the sites with $n_{\mathrm{Br}} = \pm6$, one pair of Bi atoms would provide two electrons for one ε_+ level with $n_{\mathrm{Br}} = -6$. Putting the Pb atoms on the sites with small values of $|n_{\mathrm{Br}}|$, the energy difference between the highest occupied and the lowest unoccupied cluster levels is as large as possible. When we now switch on the suppressed hopping and reduce the enhanced hopping, banding effects of the previously isolated levels will occur, including, in general, overlap of the subbands. However, the best chance to avoid band overlap will exist for those subbands that arise from levels with the biggest energy separation. In Figs. 4(a) and 4(b) we demonstrate such a transition from isolated cluster levels to bands for the configuration of Fig. 2 and also for a rocksaltlike Pb-Bi arrangement. Only for the configuration of Fig. 2, the

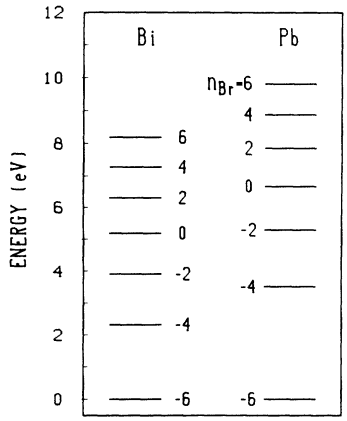

FIG. 3. Bi-O and Pb-O cluster levels for different breathing characters.

energy gap survives, for the other configuration, the gap develops at the "wrong" band filling.[17] Also note that s-like charge density is predominantly present at Bi-sites with $n_{\mathrm{Br}} = -6$ and *not* at the other Bi or Pb sites. This turns out to be a rather general observation valid for all configurations studied.

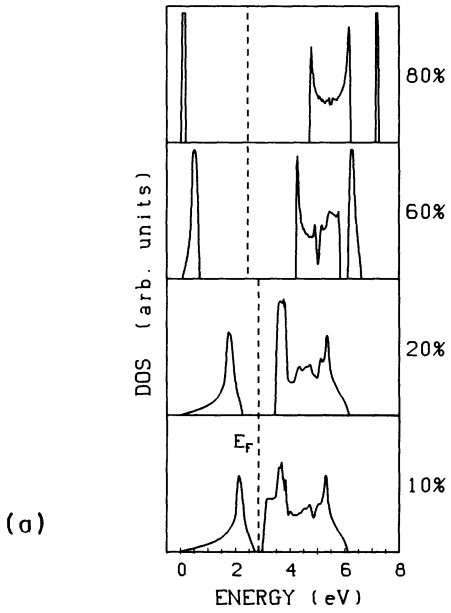

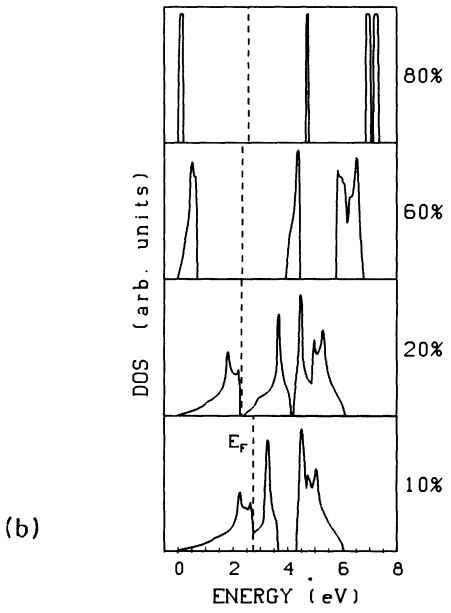

FIG. 4. (a) Banding of cluster levels for the configuration of Fig. 2. The DOS curve evolve from the case of 80% hopping asymmetry ($t^{\mathrm{short}} = 3.52$ eV, $t^{\mathrm{long}} = 0.44$ eV) to the case of 10% asymmetry ($t^{\mathrm{short}} = 2.42$ eV, $t^{\mathrm{long}} = 1.98$ eV). (b) Banding of cluster levels for a rocksalt lattice configuration of Pb and Bi.

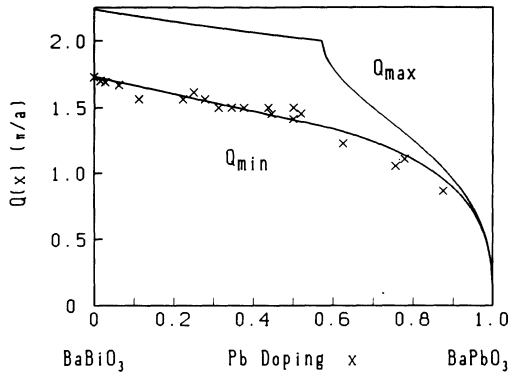

FIG. 5. $|\mathbf{Q}(x)|$ vectors of semiconducting configurations compared with the respective minimum and maximum Fermi surface diameter (solid lines) in the virtual crystal approximation.

B. Results for Ba(Bi,Pb)O_3

A large variety of configurations $\delta_{i\alpha}$ has been investigated, and nonmetallic configurations have been found over a doping range $0 \lesssim x \lesssim 0.9$. In all cases Bi and Pb atoms have been distributed according to the n_{Br} values of the sites. Other choices of the Pb/Bi distribution have always resulted in finite $N(E_F)$ values. The wave vector $\mathbf{Q}(x)$ are found to change with x in a fashion very similar to $2k_F(x)$ (see Fig. 5). Typical configurations are displayed in Fig. 6. The most important characteristics of 14 configurations are given in Table I.

For the configurations 2 ($x = 0.063$) and 12 ($x = 0.625$) of Table I, electronic density-of-states (DOS) curves are shown in Figs. 7(a) and 7(b), respectively. Also shown are the site DOS curves for the Pb, $Bi^{4+\Delta}$, and $Bi^{4-\Delta}$ sites (see the Appendix for definition of site DOS). As mentioned above, most of the charge density on the metal

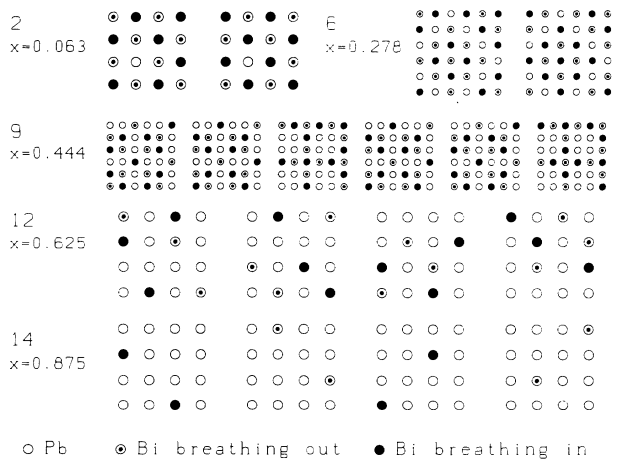

FIG. 6. Five typical semiconducting configurations. The numbering follows that of Table I. The distributions of Pb, $Bi^{4+\Delta}$, and $Bi^{4-\Delta}$ sites is indicated in the same way as in Fig. 2. The various layers of a superstructure are shown in sequence.

sites is situated at the breathing-out $Bi^{4-\Delta}$ sites.

Note that a considerable number of configurations $\delta_{i\alpha}$ has been found, which exhibit a very pronounced minimum in the $N(E)$ curve near E_F, yet do not show a complete gap. For some of these configurations, it has been tested whether slightly enhanced gradients β of the $t_{sp\sigma}$ hopping matrix element cause a complete gap at E_F. This was true, in fact, for most of these cases. In all above calculations, the modulation of ε(Bi,Pb) with breathing character has been ignored. When this modulation was implemented at a later state of our study, even bigger gaps at E_F have been obtained for the respective configurations.

Although the construction principle for the configurations $\delta_{i\alpha}$ is based on $2k_F(x)$; i.e., reciprocal space properties, there appear very distinct real-space features. For smaller doping ($x \lesssim 0.3$) chainlike structures are present, the chains being formed by the minority Pb atoms. In configurations like these, the Bi regions locally still form the distorted $Ba_2Bi^{4+\Delta}Bi^{4-\Delta}O_6$ structure, including the typical large gap at E_F, yet the chains, consisting of the minority Pb atoms, produce "impurity" bands in this gap [see Fig. 7(a)]. For doping values around $x \approx 0.5$, the real-space arrangement is changing into clusterlike Bi ordering. As a consequence, the electronic DOS curves no longer resemble the DOS curves of breathing distorted $BaBiO_3$ [see Fig. 7(b)]. Probably because of the small size of the supercell, configuration 10 ($x = 0.5$) is somewhat exceptional by still exhibiting Pb (and Bi) chains. When going to even higher x values, the decrease in $2k_F(x)$ will enforce the average Bi-Bi separation to increase beyond one nearest neighbor (NN) (see structures 12 and 14).

C. Results for (Ba,K)BiO_3

The nonmetallic configurations of (Ba,K)BiO_3 were found in a similar way as for Ba(Bi,Pb)O_3. In fact, we have used as a starting point the Ba(Bi,Pb)O_3 configu-

TABLE I. Compilation of typical data for 14 configurations $\delta_{i\alpha}$. Given are, in sequence, the Pb concentration x, the size of the supercell (SC), energy gap ε_g, type and number of breathing sites, their occupation by Pb or Bi, wave vectors **Q** used for constructing $\delta_{i\alpha}$ and the resulting **K** vectors of the Pb-Bi ordering waves. Configurations shown in Fig. 6 are denoted by an asterisk. Configuration 10 is displayed in Fig. 2.

Conf.	x	SC	ε_g [eV]	$\lvert n_{Br}\rvert$	Number	Occ.	**Q**	**K**
1	0.016	$8\times8\times2$	0.46	6, 5	122, 4	Bi	(111)	Diffuse
				2	2	Pb	$(\frac{3}{4}11), (1\frac{3}{4}1)$	
2*	0.063	$4\times4\times2$	0.33	6,5	26,4	Bi	(111)	Diffuse
				2	2	Pb	$(1\frac{1}{2}1), (\frac{1}{2}11)$	
3	0.111	$6\times6\times2$	0.10	6,4	40,24	Bi	$(11\pm\frac{2}{3}), (1\pm\frac{2}{3}1)$	$(\frac{1}{3}00), (\frac{2}{3}00)$
				2	8	Pb	$(\pm\frac{2}{3}11)$	+ others
4	0.222	$6\times6\times2$	0.19	6,4	40,16	Bi	$(1\frac{2}{3}1)$	$(\frac{2}{3}00)$
				2	16	Pb	$(\pm\frac{2}{3}11)$	$(\frac{2}{3}\frac{2}{3}0)$
5	0.25	$4\times4\times2$	0.10	6,5,4	12,8,4	Bi	(111)	(110)
				2,0	4,4	Pb	$(\frac{1}{2}11), (1\frac{1}{2}1)$	
6*	0.278	$6\times6\times2$	0.33	6,4	36,16	Bi	$(1\frac{2}{3}1)$	(110)
				2,0	8,12	Pb	$(\pm\frac{2}{3}11)$	$(\frac{1}{3}\frac{1}{3}0), (\frac{2}{3}\frac{2}{3}0)$
7	0.344	$4\times4\times4$	0.17	6,5,4	26,8,8	Bi	$(11\frac{1}{2}), (1\frac{1}{2}1)$	(001),(110)
				2,1,0	6,8,8	Pb	$(\frac{1}{2}11)$	(111)
8	0.375	$4\times4\times2$	0.29	6,5	4,16	Bi	$(1\frac{1}{2}1)$	(110)
				2,0	4,8	Pb	$(\frac{1}{2}11)$	
9*	0.444	$6\times6\times6$	0.48	6	120	Bi	$(11\frac{1}{3}), (1\frac{1}{3}1)$	$(0\frac{2}{3}\frac{2}{3}), (\frac{2}{3}\frac{2}{3}\frac{2}{3})$
				2	96	Pb	$(\frac{1}{3}11)$	+ others
10	0.5	$2\times2\times2$	0.25	6	4	Bi	(101)	(110)
				0	4	Pb	(011)	
11	0.519	$6\times6\times6$	0.24	6	104	Bi	$(11\pm\frac{1}{3}), (1\pm\frac{1}{3}1)$	$(00\frac{2}{3})$
				2,0	96,16	Pb	$(\pm\frac{1}{3}11)$	$(\frac{2}{3}0\frac{2}{3}), (\frac{2}{3}\frac{2}{3}0)$
12*	0.625	$4\times4\times4$	0.27	6	24	Bi	$(1\frac{1}{2}\frac{1}{2})$	$(\frac{1}{2}\frac{1}{2}1)$
				4,0	8,32	Pb	$(\frac{1}{2}1\frac{1}{2})$	
13	0.778	$6\times6\times6$	0.31	6	48	Bi	$(1\frac{1}{3}-\frac{1}{3}), (\frac{1}{3}1\frac{1}{3})$	$(\frac{2}{3}-\frac{2}{3}-\frac{2}{3})$
				2,0	120,48	Pb	$(\frac{1}{3}\frac{1}{3}1)$	$(\frac{2}{3}0\frac{2}{3}), (\frac{2}{3}\frac{2}{3}0)$
14*	0.875	$4\times4\times4$	0.14	6	8	Bi	(100),(010)	(110),(101)
				3,0	32,24	Pb	$(001), (\frac{1}{2}\frac{1}{2}\frac{1}{2})$	(011)

rations in the respective doping range. For $0 \lesssim x \lesssim 0.4$, most of the configurations exhibit chain structures and could be constructed within $n^2 \times 2$ superlattices. Focusing on these, we were able to find five semiconducting configurations with $x \lesssim 0.35$. It was essential for finding any gap away from $x = 0$ to include the change of ε_s(Bi) due to the respective breathing environment of the Bi site. In Fig. 8, the DOS curves for all five cases are displayed. For small x, the DOS curves are very similar to that of $BaBiO_3$. Like in the Pb-doped configurations, there appear impurity bands in the gap of the $BaBiO_3$ DOS curve.

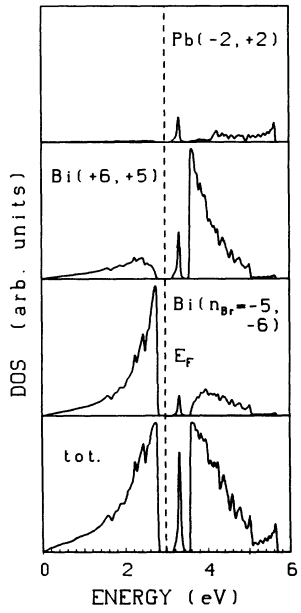

(a)

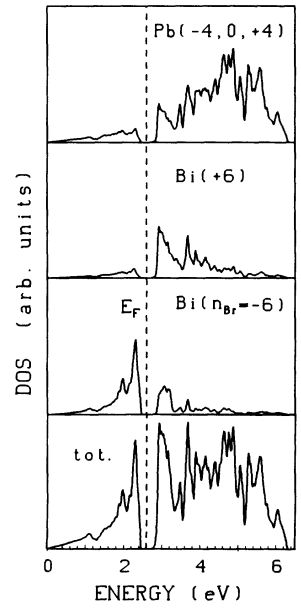

(b)

FIG. 7. (a) Site and total DOS curves for configuration 2 of Table I ($x = 0.063$). Note the midgap states, typical for all configurations with small x values. (b) Site and total DOS curves for configuration 12 of Table I (x=0.625).

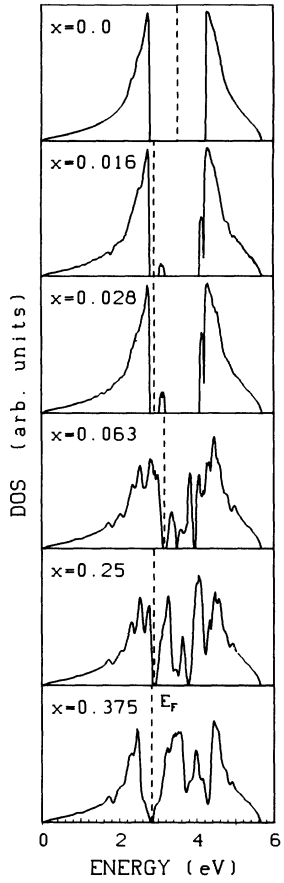

FIG. 8. Total DOS curves for pure $BaBiO_3$ and for the five semiconducting configurations of $Ba_{1-x}K_xBiO_3$.

In general, the chainlike structures are dominated by a combination of wave vector $\mathbf{Q}_1 = (1,1,1)$ and $\{\mathbf{Q}_2\} = (\frac{n-1}{n}, 1, 1)$, as is the case for the corresponding Pb-Bi configurations. In addition, further wave vectors had to be added, in particular $\mathbf{Q}_2 = (1,1,0)$. As a consequence, the corresponding configurations of Ba(Bi,Pb)O_3 and (Ba,K)BiO_3 do show significant differences, as is indicated in Fig. 9. It appears that the (Ba,K)BiO_3 con-

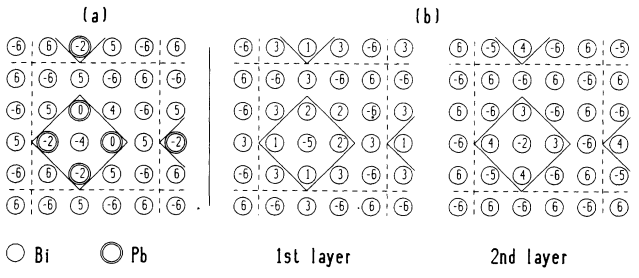

FIG. 9. Comparison of configuration 5 of Table I (x=0.25) (a) with the corresponding (Ba,K)BiO_3 configuration (b). Only one layer of the Pb/Bi configuration is shown (the other layer exhibits antisymmetric n_{Br} values). The antisite domains are indicated by solid lines. Note that in the second layer of (Ba,K)BiO_3, the antisite domain is much less pronounced than in the first layer.

figurations have the tendency to exhibit antiphase domains on the previous Pb sites. Further, while for the Ba(Bi,Pb)O_3 configurations the two layers of the $n^2 \times 2$ superstructures have been found to be antisymmetric with respect to the n_{Br} values of the sites [Fig. 9(a)], this is no longer the case for the (Ba,K)BiO_3 configuration [Fig. 9(b)].

D. Reciprocal space analysis

All configurations $\delta_{i\alpha}$ presented in our study should lead to additional Bragg peaks. If, however, the size of the superlattice domains is not very large, the intensity maxima should be broadened considerably. Yet these maxima should appear in specific regions of the Brillouin zone. Both the O distortion waves and the Pb/Bi ordering waves are origins for maxima. Therefore, we have studied both effects, using a very simple model, where the atomic form factors of O and Pb or Bi have been described by δ-functions. As expected, the O distortion waves cause maxima in accordance with the $\mathbf{Q}(x)$ vectors used to generate the respective configuration $\delta_{i\alpha}$. For the Bi-rich alloys ($x \lesssim 0.5$) the maxima thus show up in particular along the line $(1,1,\xi)$ with $1 \gtrsim \xi \gtrsim 0$, while for Pb-rich alloys ($x \gtrsim 0.5$), the maxima appear in the plane $(1,\xi,\eta)$.

On the other hand, the maxima $\mathbf{K}$ of the Pb/Bi ordering waves, in general, do not coincide with the $\mathbf{Q}(x)$ vectors (see Table I). In particular, in the Bi-rich alloys, with $\mathbf{Q}(x) = (1,1,\xi)$, the Pb/Bi ordering vectors have the forms $(2\xi, 2\xi, 0)$ as well as $(2\xi, 2\xi, 2\xi)$ and $(2\xi, 0, 0)$. The reason for doubling of ξ may be seen by considering one single breathing distortion wave of wave-number component ξ. As the Bi atoms are placed both on the maxima and minima of the distortion wave, while the Pb atoms are positioned on sites with small distortions, we obtain a doubling of the wave number for the ordering wave. For $\xi = 1$, only breathing-in or breathing-out sites are possible, so that no Pb atoms can be positioned. These components thus drop out. Superposition of various distortion waves will then preferentially lead to the forms $(2\xi, 2\xi, 0)$, etc.

E. Experimental consequences

As we have found many nonmetallic configurations with similar doping values x, we expect the real crystal to consist of many small domains of competing superstructures (of order 50 – 100 Å linear dimensions) and also fluctuations of dopant concentrations over this range. Distinct superlattice Bragg peaks should not be present. We also do not expect one specific incommensurate wave vector to dominate. Instead we predict broad maxima in the diffuse elastic scattering, caused by the proposed Pb-Bi ordering waves and O distortion waves. The maxima due to the O distortion waves are directly related to $2k_F(x)$. For doping values $x \lesssim 0.5$, the maxima should show up especially along the line $(1,1,\xi)$. Possibly, the O distortion waves cannot be detected by x-ray scattering, but only by neutron scattering, which would require relatively large single crystals. For $x \lesssim 0.5$ the Pb-Bi ordering waves should lead to maxima lying mainly in the plane $(2\xi, 2\eta, 0)$, with some preference for the line $(2\xi, 2\xi, 0)$. In order to detect the maxima in diffuse elastic scattering probably either neutron scattering or x-ray scattering using tunable x-ray sources are necessary. It is not clear to us whether electron scattering can be used (problems of surface versus bulk, sample degradation, etc.). It might be possible that the electron diffraction results of Pei *et al.*,[18] who observe an incommensurate structural modulation along the $(1,1,0)$ cubic direction for $(Ba_{1-x}K_x)BiO_3$, are related to our findings; they could be interpreted as $Bi^{4-\Delta}/Bi^{4+\Delta}$ ordering waves. However, the effect may also be induced by electron beam heating.[19]

Another consequence of our model is that two different kinds of Bi-O and Pb-O bond-length distributions are predicted. As the Bi atoms are placed either on breathing-in or on breathing-out sites, two maxima should be observed for the Bi-O bond-length distribution. On the other hand, there should exist only one maximum for the Pb-O case. Such bimodal versus unimodal bond-length distributions have indeed been observed by extended x-ray-absorption fine-structure (EXAFS) measurements.[20–22]

V. CONCLUDING REMARKS

Our model is able to give a simple explanation for the nonmetallic behavior over wide doping ranges both for $BaBi_{1-x}Pb_xO_3$ and for $Ba_{1-x}K_xBiO_3$. Starting point is the idea that breathing-type modulations of the O atoms exist, whose wave vectors change with doping x according to $2k_F(x)$ of the virtual crystal conduction band. For the Bi-Pb system, Pb-Bi ordering waves on the octahedral sites are generated by decorating the sites of strong breathing character with Bi atoms, while the remaining sites are left for Pb atoms.

Although our starting point has been the virtual crystal conduction band, the resulting electronic structures are strongly modified by the O distortion and the Pb-Bi ordering waves. On the Pb-Bi lattice, the additional charge density is mainly situated on the breathing-out $Bi^{4-\Delta}$ sites, and only to a much lesser extent on the $Bi^{4+\Delta}$ or Pb sites. This observation casts doubts on results, where the virtual crystal approximation has been used for calculating quantities like $N(E_F)$, electron-phonon coupling or superconducting properties.

Although the $2k_F(x)$ construction rule is based on reciprocal space, the resulting superstructures do exhibit distinctly different real-space features as a function of x. In particular, for small x, predominantly chainlike structures are found. The latter structures have been the basis for the search of corresponding nonmetallic $Ba_{1-x}K_xBiO_3$ configurations. It was found that there, the Pb sites are replaced by small Bi antiphase domains.

Our criterium for a nonmetallic configuration has been to find a real gap at the Fermi energy. In fact, this criterium may be too restrictive. Because of localization effects configurations exhibiting finite, yet small $N(E_F)$

values might also be nonmetallic.

Our model results in some definite experimental predictions. First we expect a bimodal distribution of Bi-O bond lengths, in contrast to a unimodal one for the Pb-O bond. Indeed, EXAFS data agree with this prediction. However, the decisive test for the validity of our model will be the experiments probing the diffuse elastic scattering of $(Ba_{1-x}K_x)BiO_3$ and $Ba(Bi_{1-x}Pb_x)O_3$ alloys.

Note added. In a recent paper by Namatame *et al.*,[23] photoemission and oxygen core level spectroscopy have been used to study the electronic structure of $BaBi_{1-x}Pb_xO_3$. The authors report that the splitting of the Bi $6s$ band is not significantly reduced by Pb substitution in the semiconducting phase. It is also found that Pb remains tetravalent and does not supply the Bi-O network with extra holes. These findings agree very well with the results of our model.

ACKNOWLEDGMENTS

This work was supported in part by the Minister für Wissenschaft und Forschung, Land Nordrhein-Westfalen, and by the European Community ESPRIT Project No. 3041-MESH.

APPENDIX: BLOCK DIAGONALIZATION OF THE HAMILTON MATRIX

Since our simplified tight-binding Hamiltonian includes only nearest-neighbor hopping between Bi (Pb) and O sites, the corresponding Hamilton matrix H for a supercell containing n unit cells can be written as

$$H = \begin{pmatrix} A & T_x^+ & T_y^+ & T_z^+ \\ T_x & \varepsilon(\mathrm{O})E & 0 & 0 \\ T_y & 0 & \varepsilon(\mathrm{O})E & 0 \\ T_z & 0 & 0 & \varepsilon(\mathrm{O})E \end{pmatrix}$$

A is a $(n \times n)$ diagonal matrix containing Bi (Pb) on-site energies on its diagonal, $T_{x(y,z)}$ are **k**-dependent $(n \times n)$ matrices describing the hopping between the Bi (Pb) atoms and the O atoms on the x (y, z) axis. E is the $(n \times n)$ unit matrix. One has to solve

$$\det(H - z) = 0.$$

The value of the determinant is not changed by multiplying the second (third, fourth) row of the block matrix by $-T^+_{x(y,z)}[\varepsilon(\mathrm{O}) - z]^{-1}$ from the left-hand side and adding it to the first one. Then

$$\det \begin{pmatrix} A - zE - [\varepsilon(\mathrm{O}) - z]^{-1} P & 0 & 0 & 0 \\ T_x & E' & 0 & 0 \\ T_y & 0 & E' & 0 \\ T_z & 0 & 0 & E' \end{pmatrix} = 0$$

with $P = T_x^+ T_x + T_y^+ T_y + T_z^+ T_z$ and $E' = [\varepsilon(\mathrm{O}) - z]E$. The resulting determinant for the triangular block matrix is given by

$$[\varepsilon(\mathrm{O}) - z]^{2n} \det\left[(A - zE)\,[\varepsilon(\mathrm{O}) - z] - P\right] = 0.$$

Since the determinant is a continuous function of z, the result is not only valid for $z \neq \varepsilon(\mathrm{O})$, but for $z = \varepsilon(\mathrm{O})$ as well. As a consequence there are always $2n$ dispersionless O bands.

It is easy to show that P is positive semidefinite and a matrix N fulfilling $N^2 = P$ can be written as $N = UDU^+$. U contains the eigenvectors of P in its columns, D is a diagonal matrix of the square roots of the eigenvalues of P. To find the remaining eigenvalues of H one has to solve

$$\det(\tilde{H} - z) = 0$$

with

$$\tilde{H} = \begin{pmatrix} A & N \\ N & \varepsilon(\mathrm{O})E \end{pmatrix}.$$

The numerical diagonalization of the $(2n \times 2n)$ matrix $\tilde{H}$ including the calculation of N is much faster than the diagonalization of the initial $(4n \times 4n)$ matrix H.

Both A and $\varepsilon(\mathrm{O})E$ are site diagonal, yet site i in $\varepsilon(\mathrm{O})E$ now represents a certain combination of the O sites around the Pb-Bi site i. As a consequence, we can define site-dependent density of states curves including both the Pb-Bi and the O component of site i. Such site DOS curves are shown in Fig. 7.

* Present address: Fritz-Haber-Institut, Berlin, Germany.
[1] L.F. Mattheiss, E.M. Gyorgy, and D.W. Johnson, Jr., Phys. Rev. B **37**, 3745 (1988).
[2] R.J. Cava, B. Batlogg, J.J. Krajewski, R.C. Farrow, L.W. Rupp, A.E. White, K.T. Short, W.F. Peck, and T.Y. Kometani, Nature (London) **332**, 814 (1988).
[3] A.W. Sleight, J.L. Gillson, and P.E. Bierstedt, Solid State Commun. **17**, 27 (1975); for a review, see B. Batlogg, Physica B+C **126**, 275 (1984).
[4] D.E. Cox and A.W. Sleight, Solid State Commun. **19**, 969 (1976).
[5] D.E. Cox and A.W. Sleight, in *Proceedings of the Conference on Neutron Scattering, Gatlinburg, 1976*, edited by R.M. Moon (National Technical Information Service, Springfield, Virginia, 1976), p. 45.
[6] D.T. Marx, P.G. Radealli, J.D. Jorgensen, R.L. Hitterman, D.G. Hinks, Shiyou Pei, and D. Dabrowski, Phys. Rev. B **46**, 1144 (1992).
[7] S. Tajima, S. Uchida, A. Masaki, H. Takagi, K. Kitazawa, S. Tanaka, and A. Katsui, Phys. Rev. B **32**, 6302 (1985).
[8] S. Tajima, S. Uchida, A. Masaki, H. Tagaki, K. Kitazawa, S. Tanaka, and S. Sugai, Phys. Rev. B **35**, 696 (1987).
[9] K. Kitazawa, S. Uchida, and S. Tanaka, Physica B **135**, 505 (1985).
[10] L.F. Mattheiss and D.R. Hamann, Phys. Rev. B **28**, 4227 (1983).

[11] We note that, for realistic O distortions, a complete gap at E_F is not obtained within the LDA. The level splittings are still somewhat smaller than the band dispersion between, in particular, the points L and W of the fcc Brillouin zone. We think that this shortcoming is another manifestation of the "gap problem" of LDA, where the fundamental gap is underestimated by as much as a factor of 2.

[12] L.F. Mattheiss and D.R. Hamann, Phys. Rev. Lett. **60**, 2681 (1988).

[13] W. Weber, Jpn. J. Appl. Phys. **26**, Suppl. 3, 981 (1987).

[14] U. Hahn, G. Vielsack, and W. Weber, in *Electronic Properties of High-T_c Superconductors and Related Compounds,* Springer Series in Solid State Sciences, Vol. 113, edited by H. Kuzmany, M. Mehring, and J. Fink (Springer-Verlag, Berlin, 1993), p. 434.

[15] G. Vielsack, W. Weber, P. Blaha, and K. Schwarz, in *Electronic Properties of High-T_c Superconductors and Related Compounds* (Ref. 14), p. 438.

[16] G. Vielsack, Ph.D. thesis, Universität Dortmund, 1993.

[17] L.F. Mattheiss, Jpn. J. Appl. Phys. **24**, 6 (1985).

[18] Shiyou Pei, N.J. Zaluzec, J.D. Jorgensen, B. Dabrowski, D.G. Hinks, A.W. Mitchell, and D.R. Richards, Phys. Rev. B **39**, 811 (1989).

[19] E.A. Hewat, C. Chaillout, M. Godinho, M.F. Gorius, and M. Marezio, Physica C **157**, 228 (1989).

[20] S.M. Heald, D. DiMarzio, M. Croft, M.S. Hedge, S. Li, and M. Greenblatt, Phys. Rev. B **40**, 8828 (1989).

[21] J.B. Boyce, F.G. Bridges, T. Claeson, T.H. Geballe, and J.M. Remeika, Phys. Rev. B **41**, 6306 (1990).

[22] J.B. Boyce, F.G. Bridges, T. Claeson, T.H. Geballe, G.G. Li, and A.W. Sleight, Phys. Rev. B **44**, 6961 (1991).

[23] H. Namatame *et al.*, Phys. Rev. B **48**, 16 917 (1993).